

Droplet activation properties of organic aerosols observed at an urban site during CalNex-LA

Fan Mei,^{1,7} Patrick L. Hayes,^{2,3} Amber Ortega,^{2,3} Jonathan W. Taylor,⁴ James D. Allan,^{4,5} Jessica Gilman,⁶ William Kuster,⁶ Joost de Gouw,⁶ Jose L. Jimenez,^{2,3} and Jian Wang¹

Received 5 July 2012; revised 15 February 2013; accepted 20 February 2013; published 11 April 2013.

[1] Size-resolved cloud condensation nuclei (CCN) spectra and aerosol chemical composition were characterized at an urban supersite in Pasadena, California, from 15 May to 4 June 2010, during the CalNex campaign. The derived hygroscopicity (κ_{CCN}) of CCN-active particles with diameter between 97 and 165 nm ranged from 0.05 to 0.4. Diurnal variation showed a slight decrease of κ_{CCN} from 8:00 to 16:00 (from 0.24 to 0.20), which is attributed to increasing organics volume fraction resulted from secondary organic aerosol (SOA) formation. The derived hygroscopicity distribution and maximum activated fraction of the size selected particles were examined as functions of photochemical age. The result indicates that condensation of secondary species (e.g., SOA and sulfate) quickly converted hydrophobic particles to hydrophilic ones, and during daytime, nearly every particle became a CCN at $\sim 0.4\%$ in just a few hours. Based on κ_{CCN} and aerosol chemical composition, the organic hygroscopicity (κ_{org}) was derived, and ranged from 0.05 to 0.23 with an average value of 0.13, consistent with the results from earlier studies. The derived κ_{org} generally increased with the organic oxidation level, and most of the variation in κ_{org} could be explained by the variation of the organic O : C atomic ratio alone. The least squares fit of the data yielded $\kappa_{\text{org}} = (0.83 \pm 0.06) \times (\text{O:C}) + (-0.19 \pm 0.02)$. Compared to previous results based on CCN measurements of laboratory generated aerosols, κ_{org} derived from measurements during the CalNex campaign exhibited stronger increase with O : C atomic ratio and therefore substantially higher values for organics with average O : C greater than 0.5.

Citation: Mei, F., P. L. Hayes, A. Ortega, J. W. Taylor, J. D. Allan, J. Gilman, W. Kuster, J. de Gouw, J. L. Jimenez, and J. Wang (2013), Droplet activation properties of organic aerosols observed at an urban site during CalNex-LA, *J. Geophys. Res. Atmos.*, 118, 2903–2917, doi:10.1002/jgrd.50285.

1. Introduction

[2] Atmospheric aerosols can directly influence the global energy budget, by scattering and absorbing incoming solar radiation [Jacobson, 2001]. Acting as cloud condensation nuclei (CCN), aerosol particles also indirectly affect the

climate by changing the microphysical structure, lifetime, and coverage of clouds. An increase in aerosol concentration will lead to a decrease of cloud droplet size and therefore enhancement of cloud albedo. This effect is known as the first indirect aerosol effect or Twomey effect [Twomey, 1977]. The smaller cloud droplet size resulting from the increased aerosol concentration also inhibits precipitation, leading to an increase in cloud lifetime and coverage (the second indirect aerosol effect) [Albrecht, 1989]. Although it is widely accepted that the Twomey and the cloud lifetime effects act to cool the Earth-atmosphere system by increasing cloud albedo, thickness, and coverage, the magnitudes of the indirect aerosol effects are poorly understood. The Intergovernmental Panel on Climate Change [IPCC, 2007] considers the indirect effects of aerosols the most uncertain components in forcing of climate change over the industrial period.

[3] One key aerosol property for understanding aerosol indirect effects is the ability of aerosol particles to form cloud droplets at atmospherically relevant supersaturations (i.e., CCN activity). For particles consisting of typical atmospheric inorganic compounds, their CCN activity is well understood and can be effectively predicted using

Additional supporting information may be found in the online version of this article.

¹Brookhaven National Laboratory, Upton, New York, USA.

²Cooperative Institute for Research in Environmental Sciences, Boulder, Colorado, USA.

³Department of Chemistry and Biochemistry, University of Colorado, Boulder, Colorado, USA.

⁴School of Earth, Atmospheric and Environmental Sciences, University of Manchester, Manchester, UK.

⁵National Centre for Atmospheric Science, University of Manchester, Manchester, UK.

⁶NOAA Earth System Research Laboratory, Boulder, Colorado, USA.

⁷Pacific Northwest National Laboratory, Richland, Washington, USA.

Corresponding author: J. Wang, Brookhaven National Laboratory, 75 Rutherford Dr, Bldg. 815E, Upton, NY 11973, USA. (jian@bnl.gov)

©2013. American Geophysical Union. All Rights Reserved.
2169-897X/13/10.1002/jgrd.50285

Köhler theory [Köhler, 1936] based on physicochemical properties of the solute, such as its mass, molar volume, and activity coefficient. However, atmospheric aerosols often contain hundreds of organic species, which can contribute ~20–90% to the total fine aerosol mass [Kanakidou et al., 2005; Zhang et al., 2007]. Depending on their properties, organic species can significantly influence the ability of aerosol particles to act as CCN and form cloud droplets [McFiggans et al., 2006]. Organic species such as organic acids can contribute solutes, facilitating the formation of cloud droplets [Shulman et al., 1996; Laaksonen et al., 1998]. Organic surfactants can increase CCN activity by reducing surface tension relative to pure water. All other things being equal, a lower surface tension leads to a smaller Kelvin effect, hence lowering critical supersaturation [Shulman et al., 1996; Facchini et al., 1999; Charlson et al., 2001; Mircea et al., 2002; Nenes et al., 2002; Lohmann et al., 2004].

[4] One key parameter that links the thermodynamic properties of aerosol species to their CCN activity, and eventually to aerosol indirect effects, is the hygroscopicity. Several essentially equivalent single parameter frameworks have been proposed to model the CCN activation and hygroscopicity of multi-component aerosols [Hudson and Da, 1996; Rissler et al., 2006; Petters and Kreidenweis, 2007; Wex et al., 2007; Petters and Kreidenweis, 2008]. These single parameter frameworks combine many of the thermodynamic details necessary for the description of water activity and provide a more streamlined approach to represent CCN activation in models. Here we will use the hygroscopicity parameter κ proposed by Petters and Kreidenweis [2007, 2008], which combines a number of factors, including solubility and surface tension, into a single hygroscopicity parameter κ which can be conveniently derived from size-resolved CCN measurements. Besides droplet activation, hygroscopicity also describes particle growth under sub-saturated conditions and is derived from particle growth factor (GF) measured by Humidified Tandem Differential Mobility Analyzer (HTDMA). Previous studies suggest that particles may exhibit larger κ values for droplet activation (derived from CCN measurements under supersaturated conditions) than that for particle growth (derived from particle GF under sub-saturated conditions) [Duplissy et al., 2008; Wex et al., 2008; Petters et al., 2009b; Wex et al., 2009; Good et al., 2010]. In this paper, unless otherwise noted, “hygroscopicity” refers to κ associated with droplet activation under supersaturated conditions.

[5] In recent years, many studies have examined the CCN activity and hygroscopicity of laboratory-generated organic aerosols (OA) with known composition, including single compound and controlled mixtures of a few compounds [Raymond and Pandis, 2002; Kumar et al., 2003; Raymond and Pandis, 2003; Bilde and Svenningsson, 2004; Abbatt et al., 2005; Huff-Hartz et al., 2006; Svenningsson et al., 2006]. While these studies provide important insight into the ability of organics to form cloud droplets, ambient aerosols are much more complex mixtures often consisting of hundreds of species. Secondary organic aerosols (SOA) generated in controlled environmental chambers and aerosol generated in laboratory biomass burning experiments are more representative of ambient OA, and their hygroscopicities have been increasingly studied in recent years

[Hegg et al., 2001; Abbatt et al., 2005; Hartz et al., 2005; VanReken et al., 2005; King et al., 2007; Prenni et al., 2007; Duplissy et al., 2008; Engelhart et al., 2008; Asa-Awuku et al., 2009; King et al., 2009; Petters et al., 2009a; Wex et al., 2009; Massoli et al., 2010; Duplissy et al., 2011; Lambe et al., 2011]. A number of field studies also reported the range of κ for the organic component of ambient aerosols [Shantz et al., 2008; Gunthe et al., 2009; Jimenez et al., 2009; Chang et al., 2010; Rose et al., 2010]. Collectively, the laboratory and field studies suggest that organics have a fairly wide range of κ values ranging from 0 to 0.3, and κ of organic species can increase substantially during their chemical aging [Jimenez et al., 2009; Massoli et al., 2010; Duplissy et al., 2011; Lambe et al., 2011].

[6] The sensitivity of predicted CCN concentration and droplet number concentration to aerosol properties, including the hygroscopicity of organic species, are examined in a number of recent studies [Rissman et al., 2004; McFiggans et al., 2006; Wang, 2007; Wang et al., 2008; Reutter et al., 2009; Ervens et al., 2010; Kammermann et al., 2010; Ward et al., 2010]. While these studies all recognize the importance of particle size distribution, mixing state, and volume fraction of organics in particles, they also indicate that the predicted CCN concentration and droplet number concentration can be very sensitive to the hygroscopicity of organics (hereafter κ_{org})—and the value of κ_{org} needed to reproduce the measured CCN concentration can vary substantially—and depends on the location and time of the study. Using a constant κ_{org} may lead to significant biases in predicted CCN concentrations. A recent study based on the NCAR Community Atmospheric Model (CAM) shows that even modest changes in the κ_{org} of primary OA (POA) or SOA (i.e., increase of POA κ_{org} from 0 to 0.1 or decrease of SOA κ_{org} from 0.14 to 0.07) can lead to significant changes in simulated CCN concentrations and an uncertainty range of 0.4 W/m² in global average aerosol indirect forcing [Liu and Wang, 2010]. This uncertainty is comparable, or even greater than the uncertainty due to the parameterization of some of the very important cloud physics processes, such as autoconversion [Liu et al., 2008]. These studies suggest that κ_{org} needs to be better understood and represented in future climate models in order to reduce the uncertainty in simulated aerosol CCN concentrations.

[7] As described earlier, using a constant (i.e., static) κ_{org} for all organics leads to large uncertainty in simulated CCN concentration and aerosol indirect effects. At the same time, due to computational constraints, the hundreds of organic species in atmospheric aerosols and their hygroscopicities cannot be simulated individually in global models. Furthermore, the hygroscopicities of many organic species observed in ambient aerosols are often not available to predict their cloud-activation behavior using Köhler theory. Therefore, efficient parameterizations that can capture the major variation of κ_{org} are essential for implementation in large scale models. One promising idea is that the κ_{org} under both supersaturated and sub-saturated conditions may be parameterized based on the organic oxidation level (e.g., O:C atomic ratio), which can be measured by aerosol mass spectrometers (AMS) [Jimenez et al., 2009] and other techniques. For particle hygroscopic growth under subsaturated conditions, κ_{org} derived from particle GF increases with O:C

for a number of OA [Jimenez *et al.*, 2009; Massoli *et al.*, 2010; Duplissy *et al.*, 2011]. Similar correlations were also found for hygroscopicity under supersaturated conditions. Massoli *et al.* [2010] and Lambe *et al.* [2011] studied the hygroscopicity of SOA and oxidized POA generated from a variety of precursors representing atmospherically relevant biogenic and anthropogenic sources using a Potential Aerosol Mass (PAM) flow reactor [Kang *et al.*, 2007]. They found that to first order, κ_{org} is well represented by a linear function of O:C atomic ratio. Chang *et al.* [2010] studied the relationship between κ_{org} and O:C ratio for aerosols observed at a rural site in Canada, and the result is consistent with finding that κ_{org} increases with O:C ratio. At present, the data on the hygroscopicity of ambient organics are scarce, and the relationship between κ_{org} and O:C ratio needs to be examined for ambient aerosols from representative OA sources before it can be confidently implemented in climate models. In this paper, we report particle hygroscopicity and mixing state derived from size-resolved CCN measurements carried out during CalNex campaign for air masses with a range of photochemical ages. Organic hygroscopicity was derived from particle chemical composition and particle hygroscopicity, and its relationship to organics oxidation level is discussed.

2. Experimental Method

2.1. Measurement Site

[8] CalNex was a field campaign focusing on the characterization of atmospheric processes over California and the eastern Pacific coastal region in 2010 (<http://www.esrl.noaa.gov/csd/projects/calnex/>). Aerosol measurements were taken at the CalNex-LA supersite located on the California Institute of Technology (Caltech, 34°8'26.10"N, 118°7'20.84"W) campus in Pasadena from 15 May to 15 June 2010. The data related to the analyses presented in this paper were available from 15 May to 4 June. The site was near a combination of residential and commercial areas and is 15 km northeast (NE) of downtown Los Angeles. Aerosol data included aerosol size distribution, chemical composition, CCN spectrum (as a function of supersaturation), size-resolved CCN spectrum, and activated fraction, all of which were taken at the ground level (236 m above mean sea level). All measurements are reported at ambient conditions and local time (UTC time minus 7 h) throughout this study.

2.2. Size-Resolved CCN Spectrum and Activated Fraction

[9] The size-resolved CCN Spectrum and activated fraction were measured by a scanning mobility particle sizer (SMPS) and a cloud condensation nuclei counter (CCN counter) operated in series [Frank *et al.*, 2006; Petters *et al.*, 2007; Moore *et al.*, 2010]. By isolating the influence from particle size, size resolved CCN measurements provide unique insights into particle composition and mixing state, and their impacts on the particle CCN activity [Lance, 2007; Gunthe *et al.*, 2009; Petters *et al.*, 2009a; Asa-Awuku *et al.*, 2010; Mochida *et al.*, 2010; Padro *et al.*, 2010; Rose *et al.*, 2010; Irwin *et al.*, 2011; Padro *et al.*, 2012]. The instrumentation setup is shown in Figure 1. Ambient aerosol was first dried to below 20% relative humidity and neutralized by a Kr-85 aerosol neutralizer (TSI, 3077A),

and subsequently classified by a differential mobility analyzer (DMA, TSI 3081). The classified aerosol was then simultaneously characterized by a condensation particle counter (CPC, TSI 3771) and a cloud condensation nuclei counter (DMT, single column CCN counter) [Roberts and Nenes, 2005; Lance *et al.*, 2006; Rose *et al.*, 2008]. The size of classified aerosol particles was scanned between 20 and 350 nm [Wang and Flagan, 1990], while the supersaturation inside the CCN counter was held constant. The aerosol size distribution was derived by inverting the particle concentration measured by the CPC using a routine described in Collins *et al.* [2002], which explicitly accounts for multiply charged particles. The same procedure was also applied to measured CCN concentration to obtain size-resolved CCN activated fraction (number fraction of particles that serve as CCN under the supersaturation as a function of particle size).

[10] During CalNex, the sample and sheath flows of the DMA were maintained at 0.8 and 8 L min⁻¹, respectively. The total flow of CPC3771 was reduced to 0.5 L min⁻¹, and the sample flow of the CCN counter was maintained at 0.3 L min⁻¹. The measurement sequence is illustrated in Figure 2. The longitudinal temperature gradient of the CCN counter was stepped through 3.8, 4.5, 5.5, 6.5, 8, and 10°C (Figure 2b), which corresponded to supersaturations (*S*) of 0.08%, 0.13%, 0.18%, 0.22%, 0.29%, and 0.38%, respectively. The supersaturation inside the CCN counter was maintained at each value for approximately 20 min, during which the diameter of particles classified by the DMA was scanned between 20 nm and 350 nm four times (310 s per scan) [Wang and Flagan, 1990]. Immediately following each change of temperature gradient (i.e., supersaturation), the system waited for 100 s to ensure that the temperatures stabilized before the next scan of particle size commenced. The CCN counter was stepped through the above six *S* values approximately every 2 h.

[11] The CCN counter was calibrated for the 0.3 L min⁻¹ sampling flow rate and under the six temperature gradients using ammonium sulfate at the CalNex-LA site both before and after the study. The instrument supersaturations were derived from Köhler theory using a constant van't Hoff factor of 2.5 for ammonium sulfate. Since both sample pressure and temperature were essentially identical during measurements and calibrations, no correction of the calibrated supersaturation was necessary.

2.3. Measurement of Total CCN Concentrations

[12] In addition to size-resolved CCN spectrum and activated fraction, total CCN concentration was measured using a second DMT CCN counter operated at a flow rate of 0.3 L min⁻¹, and longitudinal temperature gradients of 4.7, 5.6, 6.6, 8, and 10.1°C. Based on calibrations using ammonium sulfate particles, the corresponding supersaturations derived from Köhler theory using a constant van't Hoff factor of 2.5 were 0.15%, 0.19%, 0.23%, 0.30%, and 0.39% for the five temperature gradients. The temperature gradient was stepped through the five values as shown in Figure 2a. At each value, the temperature gradient was maintained for 4 min except for that at 0.15%, when an additional 10 min was included (i.e., total 14 min) because it took substantially longer time for temperatures to reach their set points when

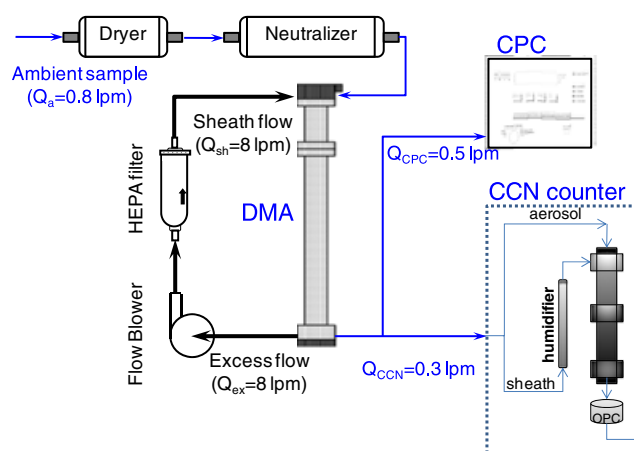


Figure 1. Setup of the size-resolved cloud condensation nuclei spectrum and activated fraction measurements.

the gradient was reduced from 10.1°C to 4.7°C. Data collected before temperatures had stabilized following changes of the temperature gradient were excluded from analysis. Same as size-resolved CCN measurements, both sampling pressure and temperature were practically identical between calibration and measurements.

2.4. Chemical Composition

[13] The concentrations of submicron non-refractory (NR-PM₁) organic and inorganic (nitrate, sulfate, ammonium) aerosol particles were measured using a high-resolution time-of-flight aerosol mass spectrometer (HR-ToF-AMS, Aerodyne Research Inc., hereinafter AMS for short) [DeCarlo *et al.*, 2006]. The AMS sampled from an inlet equipped with a PM_{2.5} cyclone located 2 m above the roof of the container housing the instrument. The ambient air passed through a 6.8 m insulated copper inlet line and a drier prior to sampling by the AMS. The resulting data was averaged over 2.5 min intervals. All data were analyzed using standard AMS software (SQUIRREL v1.51 and PIKA v1.10) within Igor Pro 6.2.1 (Wave Metrics, Lake Oswego, OR) [Sueper, 2011].

High-resolution analysis of the mass spectra was carried out following previously published procedures [Aiken *et al.*, 2007; Aiken *et al.*, 2008; Hayes *et al.*, 2012]. The aerosol organics were classified into different components using Positive Matrix Factorization (PMF), including hydrocarbon-like organic aerosol (HOA), and two types of oxygenated organic aerosols (OOA) [Hayes *et al.*, 2012].

[14] Refractory black carbon (referred to as BC in this study) mass concentration was measured using a single particle soot photometer (SP2, Droplet Measurement Technologies, Boulder, Colorado, USA). Particles are drawn through a high-intensity 1064 nm intracavity neodymium:yttrium/aluminum/garnet laser which is strongly absorbed by BC-containing particles, causing them to heat to incandescence as they evaporate [Stephens *et al.*, 2003]. Two photomultiplier tubes detect the incandescent light on a single-particle basis, and the amount of light detected is proportional to the mass of each particle [Schwarz *et al.*, 2010]. Single particle BC mass was calibrated using glassy carbon spheres, as described by McMeeking *et al.* [2010] and Liu *et al.* [2010]. The SP2 detects BC in the range

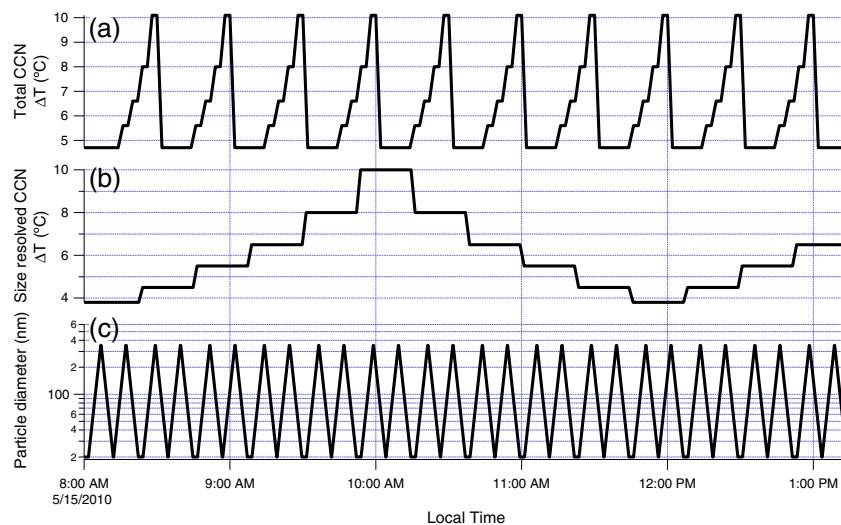


Figure 2. An example of measurement sequence for (a) temperature gradient of the CCN counter for total CCN concentration measurements, (b) the CCN counter temperature gradient, and (c) the particle diameter classified by DMA for the size resolved CCN measurements.

80–500 nm mass equivalent diameter; lognormal fits to the measured BC core size distribution were used to correct for mass outside the detection range. The SP2 data were measured every second and averaged to 5 min intervals. The coated BC size distribution was estimated from the size distribution of HOA and then normalized to the bulk BC mass loading [Zhang *et al.*, 2005a; Zhang *et al.*, 2005b; Cubison *et al.*, 2008].

3. Data Overview

3.1. Diurnal Variations of Aerosol Properties

[15] Diurnal variations of aerosol properties observed during weekdays are shown in Figure 3, including aerosol

particle size distribution (Figure 3a), species mass concentrations measured by the AMS and SP2 (Figure 3b), derived volume fractions of major species (Figure 3c), and measured CCN concentrations (Figure 3d). The mass concentration of BC was typically less than $1 \mu\text{g}/\text{m}^3$, contributing to less than 5% of the total submicron aerosol volume. Sulfate and nitrate were essentially neutralized by ammonium in the CCN-relevant sizes [Hayes *et al.*, 2012]. Sulfate volume fraction was relatively constant at about 20% throughout the day. The mass concentration and volume fraction of nitrate typically peaked in the cooler mornings and decreased in the afternoon. Among all species, organics had the largest contribution to the total aerosol volume. High number concentration (N_{CN}) of Aitken mode

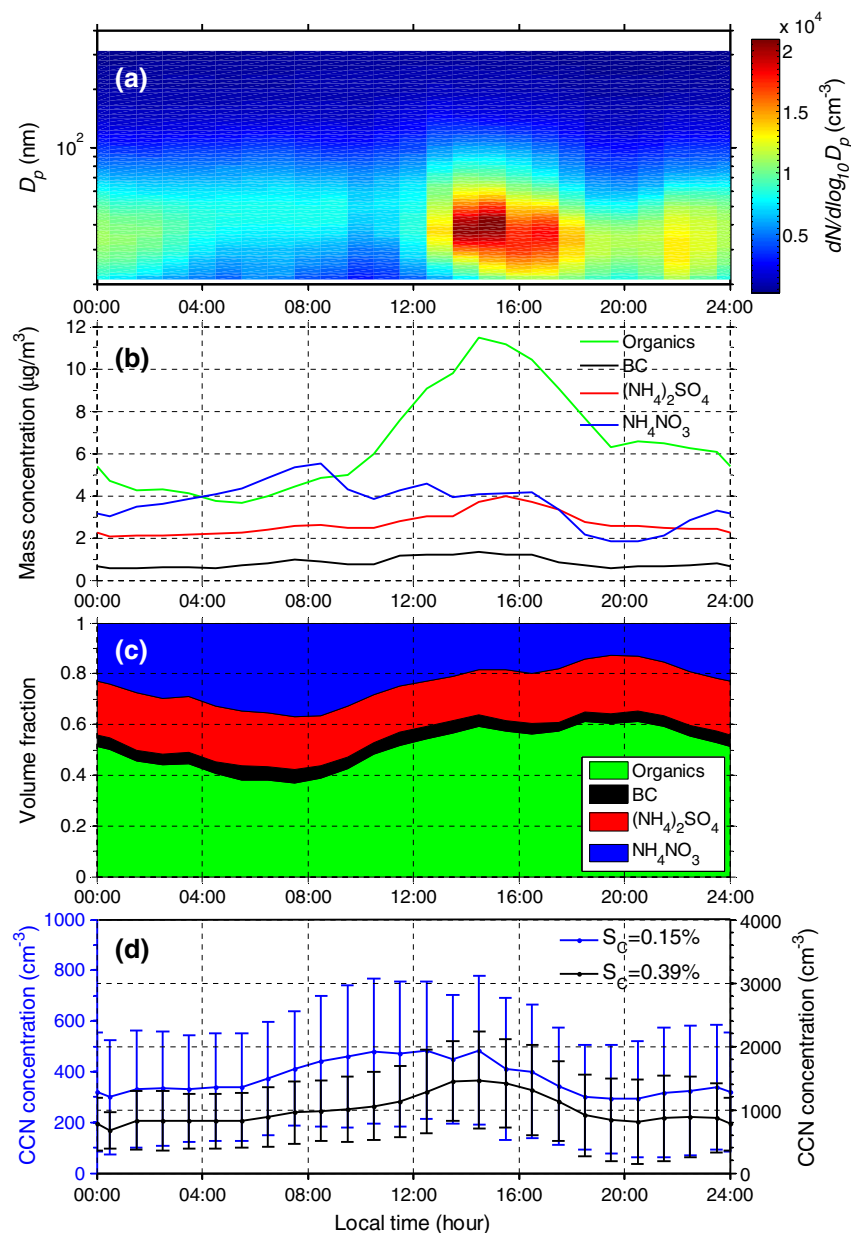


Figure 3. Diurnal variations of aerosol properties observed at the ground site during weekdays. (a) Aerosol size distribution measured by SMPS; (b) mass concentrations and (c) volume fractions of organics, black carbon, $(\text{NH}_4)_2\text{SO}_4$, and NH_4NO_3 ; and (d) CCN concentrations measured at supersaturations of 0.15% and 0.39%.

particles, CCN concentrations (N_{CCN}), and sulfate and organic mass concentration were often observed in the afternoon between 12:00 and 18:00, and are attributed to urban plume transported from downtown LA [Hersey *et al.*, 2011; Wonaschutz *et al.*, 2011; Hayes *et al.*, 2012]. The diurnal variations in mass concentration were also influenced by vertical dilution from the rising planetary boundary layer in the afternoon [Hayes *et al.*, 2012]. Due to the strong increase in organics mass concentration, organics dominated the overall composition and its volume fraction averaged over weekdays reached above 60% in the afternoon. The measured CCN concentrations under different supersaturations showed somewhat different diurnal variations. N_{CCN} at 0.39% peaked near 14:00, when organics and sulfate reached their maximum mass concentrations. Because the particle critical activation diameter is smaller under higher supersaturation, this increase was likely due to growth of small particles through condensation of hygroscopic species, including SOA and sulfate, during their transit from downtown LA [Hersey *et al.*, 2011; Wonaschutz *et al.*, 2011; Hayes *et al.*, 2012]. In comparison, N_{CCN} under lower supersaturation of 0.15% peaked earlier around noon. As larger particles tended to have larger fraction of nitrate, N_{CCN} under lower supersaturation was more influenced by nitrate concentration, which typically peaked in the cooler mornings. The oxygenated organic aerosol (OOA) was the dominant organic species, and the average OOA mass fraction was 66% for the whole campaign, suggesting SOA was a major component at this site [Hayes *et al.*, 2012]. Given the large fraction of SOA and the behavior of other species, the CalNex-LA site was principally a receptor site for pollution from downtown LA.

4. Methods

4.1. Derivation of Particle Hygroscopicity and Mixing State

[16] The impact of particle composition on CCN activity is manifested in particle hygroscopicity, which can be represented by a single parameter κ [Petters and Kreidenweis, 2007]. In this study, particle hygroscopicity κ and the mixing state were derived from the measured size-resolved CCN activated fraction using κ -Köhler theory [Petters and Kreidenweis, 2007]. In κ -Köhler theory, the water vapor saturation ratio over the aqueous solution droplet S is given by

$$S = \frac{D^3 - D_p^3}{D^3 - D_p^3(1 - \kappa)} \exp\left(\frac{4\sigma_w M_w}{RT\rho_w D}\right) \quad (1)$$

where D is the droplet diameter, D_p the dry diameter of the particle, M_w the molecular weight of water, σ_w the surface tension of pure water, ρ_w the density of water, R the gas constant, and T the absolute temperature. When κ is greater than 0.1, it can be conveniently derived as

$$\kappa = \frac{4A^3}{27D_p^3 S_c^2} \quad (2)$$

where $A = \frac{4\sigma_w M_w}{RT\rho_w D}$, and S_c is the particle critical supersaturation and was derived using the approach detailed below. Figure 4 shows an example of the activated fraction of size selected

particles as a function of supersaturation. This example is for dry particles of 142 nm in diameter measured from 8:50 P.M. to 10:50 P.M. on 4 June. The activated fraction R_a was near zero at the lowest supersaturation (0.08%) measured. R_a increased with increasing supersaturation and eventually reached a plateau of ~80%. Like this example, the maximum activated fraction at the plateau, E , was often less than 100% during CalNex, especially for particles with diameter less than 200 nm. This indicates external mixing of aerosol species for the size selected particles. The difference $1-E$ represents the number fraction of particles consisting of only non-hygroscopic species (e.g., BC) that cannot serve as CCN under typical atmospheric supersaturations.

[17] The characteristic critical supersaturation (S^*) of the size selected CCN is represented by the supersaturation at which R_a reaches 50% of E (Figure 4). The slope of R_a with respect to supersaturation near S^* provides information on the heterogeneity of the composition for the size selected particles that are CCN active. For an ideal case when all CCN-active particles have the same composition and size, a step change of R_a from 0 to E would be observed as supersaturation increases and reaches S^* . A gradual increase in R_a suggests that some of the particles have higher hygroscopicity and/or larger sizes (i.e., due to the resolution of DMA) and are able to activate at lower supersaturations than others. The activated fractions measured at the six supersaturations were fitted using both a sigmoid function [Lance, 2007; Bougiatioti *et al.*, 2011; Cerully *et al.*, 2011; Lance *et al.*, 2012; Padro *et al.*, 2012] and a lognormal function (supplementary Information), with E and S^* among fitting parameters. For each set of measurements, the function form that yielded the best fit (i.e., smaller least square residue) was used for subsequent analysis. The probability density function of the hygroscopicity of size-selected CCN was first derived based on the fitted R_a (as a function of S). The density function was then used to calculate the dispersion of CCN hygroscopicity. The dispersion of CCN hygroscopicity, which reflects the chemical heterogeneity of activated particles, is defined as $\sigma(\kappa)/\bar{\kappa}$, where $\sigma(\kappa)$ and $\bar{\kappa}$ are the standard deviation and the average of the CCN hygroscopicity, respectively. The details of the derivations are given in the auxiliary material.

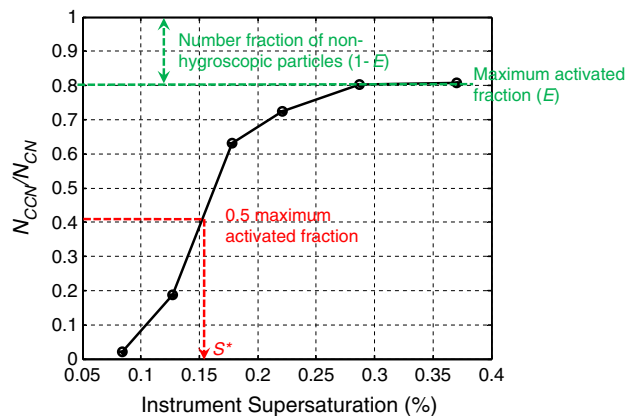


Figure 4. Activated fraction as a function of supersaturation based on measurement of particles with a diameter of 142 nm averaged from 8:50 P.M. to 10:50 P.M. on 4 June.

4.2. Derivation of Hygroscopicity of Organic Aerosol

[18] Measurements from AMS show that the composition of non-refractory submicron particles was dominated by organics, ammonium, sulfate, and nitrate. The contribution of chloride was negligible (less than 1%) [Hayes *et al.*, 2012] especially for particles within the size range of size-resolved CCN measurements. The analysis of anion and cation balance suggests that anionic species (NO_3 , SO_4) were neutralized by NH_4 over the size range relevant to CCN activation [Hayes *et al.*, 2012]. For refractory species, only BC was considered as the contribution of sea salt and dust are expected to be negligible for the size range of interest (i.e., less than 300 nm) at the CalNex-LA site. Therefore, we considered aerosols observed at the site consisting of the following four species: Organics, $(\text{NH}_4)_2\text{SO}_4$, NH_4NO_3 , and BC. For CCN observed during CalNex, the particle hygroscopicity is therefore the volume average of the four participating species:

$$\begin{aligned} \kappa_{\text{CCN}} &= \sum_i x_i \kappa_i \\ &= x_{\text{org}} \kappa_{\text{org}} + x_{(\text{NH}_4)_2\text{SO}_4} \kappa_{(\text{NH}_4)_2\text{SO}_4} + x_{\text{NH}_4\text{NO}_3} \kappa_{\text{NH}_4\text{NO}_3} \\ &\quad + x_{\text{BC}} \kappa_{\text{BC}} \end{aligned} \quad (3)$$

where x_i is the volume fraction of species i . The values of κ are 0.67 and 0.61 for $(\text{NH}_4)_2\text{SO}_4$ and NH_4NO_3 , respectively, and BC was treated as non-hygroscopic (i.e., $\kappa=0$). The hygroscopicity of CCN (κ_{CCN}) can be derived from equation (2) based on S^* :

$$\kappa_{\text{CCN}} = \frac{4A^3}{27D_p^3(S^*)^2} \quad (4)$$

and the organic hygroscopicity κ_{org} is given by subtracting the contribution of the other species from the overall CCN hygroscopicity:

$$\kappa_{\text{org}} = \frac{1}{x_{\text{org}}} \left(\kappa_{\text{CCN}} - \kappa_{\text{NH}_4\text{NO}_3} x_{\text{NH}_4\text{NO}_3} - \kappa_{(\text{NH}_4)_2\text{SO}_4} x_{(\text{NH}_4)_2\text{SO}_4} \right) \quad (5)$$

[19] The derivation of κ_{org} requires the volume fraction of $(\text{NH}_4)_2\text{SO}_4$ and NH_4NO_3 of activated size-selected particles, which were derived from size-resolved AMS measurements (particle time of flight “PToF” mode) and SP2 data described as follows. AMS and SP2 measurements were averaged into periods ranging from 2.6 to 9.0 h to increase signal-to-noise ratios (SNR). Particle chemical composition was essentially constant during the chosen periods. The selection of these averaging periods is detailed in section 5.3. This averaging was especially necessary for size-resolved mass concentrations and elemental ratios from AMS measurements because of the limited SNR arising from the low duty cycle during size-resolved measurements. Within the size range, species volume fractions at each size were derived from mass concentrations and densities of each species. The densities of $(\text{NH}_4)_2\text{SO}_4$ and NH_4NO_3 were assumed to be 1770 kg m^{-3} and 1730 kg m^{-3} , respectively. A density of 1800 kg m^{-3} was used for BC [Park *et al.*, 2004; Bond and Bergstrom, 2006]. Organics were assumed to have a density of 1200 kg m^{-3} , which is within the typical range of previous measurements [Turpin and Lim, 2001; Cross *et al.*, 2007; Malloy *et al.*, 2009; Kuwata *et al.*,

2012]. It is worth noting that a less than 100% maximum activated fraction (E) suggests that some of the size-selected particles are non-hygroscopic and do not serve as CCN under atmospherically relevant supersaturations. In this study, we assume that these non-hygroscopic particles consisted of only BC. At the size of particles classified by the DMA, the volume concentration of externally mixed BC, which represents the volume concentration of non-hygroscopic particles, was derived as the product of $(1-E)$ and the total volume concentration (i.e., the sum of volume concentrations of organics, $(\text{NH}_4)_2\text{SO}_4$, NH_4NO_3 , and BC). The volume concentration of the externally mixed BC was then subtracted from the total BC volume concentration, and the balance gave the volume concentration of BC that was internally mixed within the CCN-active particles. The volume fractions required to derive κ_{org} from equation (5) were then calculated by combining the volume concentrations of organics, sulfate, nitrate, and the internally mixed BC. As shown later, κ_{org} was derived from periods when the vast majority of particles were internally mixed and CCN-active, and the $(1-E)$ was less than 15%. In the derivation of species volume fractions at classified size, the particle vacuum aerodynamic diameter (D_{va} , measured by AMS) and particle mobility diameter (D_m , classified by DMA) were converted to particle volume equivalent diameter (D_{ve}) assuming spherical particles (For spherical particles, both D_m and D_{ve} are equal to particle geometric diameter). This assumption is reasonable except for freshly emitted, externally mixed BC particles, which are non-spherical aggregates of individual spherules produced by combustion. For fresh BC particles, the assumption of spherical particles leads to overestimate of D_{ve} from D_m and underestimate of D_{ve} from D_{va} [DeCarlo *et al.*, 2004]. Without information on BC morphology and its variation with particle size and time, it is difficult to estimate the influence of this assumption on calculated N_{CCN} . In this study, κ_{org} was derived based on hygroscopicity of CCN classified at sizes of 126, 142, 160, and 180 nm, at which both the counting statistics of size-resolved CCN measurements (based on aerosol number) and the signal to noise ratio of the AMS measurements (aerosol mass based) were reasonable.

4.3. Uncertainty Analysis for Organics Hygroscopicity Derivation

[20] Based on equation (5), the uncertainty in derived κ_{org} can be attributed to the uncertainties in κ_{CCN} and volume fractions of the participating species in the activated particles. As the volume fractions were derived from volume concentrations computed from AMS and SP2 measurements, the uncertainty of derived κ_{org} is given by (detailed derivation given in auxiliary material):

$$\begin{aligned} \sigma_{\kappa_{\text{org}}}^2 &= \left(\frac{\kappa_{\text{CCN}}}{x_{\text{org}}} \right)^2 \left(\frac{\sigma_{\kappa_{\text{CCN}}}}{\kappa_{\text{CCN}}} \right)^2 + (\kappa_{\text{inorg}} - \kappa_{\text{org}})^2 x_{\text{inorg}}^2 \left(\frac{\sigma_{v_{\text{org}}}}{v_{\text{org}}} \right)^2 \\ &\quad + (\kappa_{\text{inorg}} - \kappa_{\text{org}})^2 x_{\text{inorg}}^2 \left(\frac{\sigma_{v_{\text{inorg}}}}{v_{\text{inorg}}} \right)^2 \\ &\quad + \left(\frac{\kappa_{\text{CCN}} x_{\text{BC}}}{x_{\text{org}}} \right)^2 \left(\frac{\sigma_{v_{\text{BC}}}}{v_{\text{BC}}} \right)^2 \end{aligned} \quad (6)$$

where v_i represents the volume concentration of species i and κ_{inorg} is the average hygroscopicity of the particle inorganic component, which included $(\text{NH}_4)_2\text{SO}_4$ and NH_4NO_3 :

$$\kappa_{\text{inorg}} = \frac{\kappa_{\text{NH}_4\text{NO}_3} x_{\text{NH}_4\text{NO}_3} + \kappa_{(\text{NH}_4)_2\text{SO}_4} x_{(\text{NH}_4)_2\text{SO}_4}}{x_{\text{NH}_4\text{NO}_3} + x_{(\text{NH}_4)_2\text{SO}_4}} \quad (7)$$

[21] Note that $(\text{NH}_4)_2\text{SO}_4$ and NH_4NO_3 have very similar κ values (0.67 and 0.61, respectively); for the derivation of the uncertainty in κ_{org} , a constant value of 0.64 was used for κ_{inorg} .

[22] The first term on the right-hand side (RHS) of equation (6) is associated with the uncertainty in derived κ_{CCN} , which is due to the accuracy of the dry size of particles classified by the DMA [Wang *et al.*, 2003] and uncertainty in S^* derived from size-resolved CCN measurements during the periods (details given in auxiliary material) of this study. The second, third, and fourth terms on the RHS of equation (6) represent contributions due to the uncertainties in volume fractions of organics, inorganics, and BC, respectively. The volume fractions were derived from the average mass concentrations measured during the periods and densities of the species. For the purpose of estimating the uncertainty in species volume fractions, an uncertainty of 10% was estimated for inorganic, organic, and BC volume concentrations. The details for estimating the uncertainty are described in auxiliary material. As the volume of BC was typically very low (i.e., $\sim 10\%$ or less), especially for the periods used for derivation of κ_{org} , an increase in x_{org} led to a decrease in x_{inorg} . Therefore, equation (6) indicates that the contributions from $\sigma_{\kappa_{\text{CCN}}}$, $\sigma_{v_{\text{org}}}$, and $\sigma_{v_{\text{inorg}}}$ (the first, second, and third terms on the RHS of equation (6), respectively) decreased with increasing x_{org} . In addition, the contribution from $\sigma_{v_{\text{BC}}}$ was likely to be minor due to the low value of x_{BC} . These features are evident from the variation of $\sigma_{\kappa_{\text{org}}}^2$ and contributions from different terms as a function of x_{org} shown in Figure 5. The variation in $\sigma_{\kappa_{\text{org}}}^2$ was calculated using equation (6) assuming 10% for $\frac{\sigma_{v_{\text{org}}}}{v_{\text{org}}}$, $\frac{\sigma_{v_{\text{inorg}}}}{v_{\text{inorg}}}$, $\frac{\sigma_{v_{\text{BC}}}}{v_{\text{BC}}}$, and 0.1 for κ_{org} . As shown later, the value of κ_{org} had very minor impact on $\sigma_{\kappa_{\text{org}}}^2$. BC volume fraction and $\frac{\sigma_{\kappa_{\text{CCN}}}}{\kappa_{\text{CCN}}}$ were assumed as 10% and 7%, respectively, which are representative for the measurements at the CalNex-LA site during the study.

[23] Figure 5 shows that the contribution from $\sigma_{v_{\text{BC}}}$ (the fourth term of RHS of equation (6)) was negligible for the entire x_{org} range studied. Even when $\frac{\sigma_{v_{\text{BC}}}}{v_{\text{BC}}}$ was increased from 10% to 30%, its contribution remained less than 1.5% of overall $\sigma_{\kappa_{\text{org}}}^2$ when x_{org} was greater than 50% (not shown). The overall $\sigma_{\kappa_{\text{org}}}^2$, which was essentially the same as the combined contribution from $\sigma_{\kappa_{\text{CCN}}}$, $\sigma_{v_{\text{org}}}$, and $\sigma_{v_{\text{inorg}}}$ (i.e., sum of first three terms of equation (6)) decreased rapidly with increasing x_{org} . This variation of $\sigma_{\kappa_{\text{org}}}^2$ with x_{org} can be explained as follows. First, at lower x_{org} , κ_{org} was increasingly being derived as the difference among three large numbers, which resulted in higher uncertainty in derived κ_{org} . Second, a higher x_{org} led to smaller uncertainty in derived x_{org} . For example, at x_{org} of 100% (i.e., pure OA particles), the uncertainty in measured organics mass concentration has no impact on derived x_{org} . This is also evident from equation (6), which shows that the contributions from $\sigma_{v_{\text{org}}}$ and $\sigma_{v_{\text{inorg}}}$ were scaled to $x_{\text{inorg}}^2 \approx (1 - x_{\text{org}})^2$. Therefore, the analyses described below were focused mostly on aerosols with organic volume fraction higher than 60%,

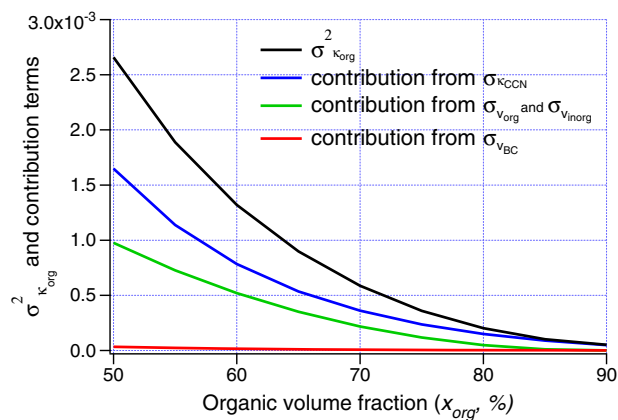


Figure 5. Variations of $\sigma_{\kappa_{\text{org}}}^2$ and contributions from different terms as functions of x_{org} . The value of $\sigma_{\kappa_{\text{org}}}^2$ was calculated using equation (6) assuming 10% for $\frac{\sigma_{v_{\text{org}}}}{v_{\text{org}}}$, $\frac{\sigma_{v_{\text{inorg}}}}{v_{\text{inorg}}}$, and $\frac{\sigma_{v_{\text{BC}}}}{v_{\text{BC}}}$, and 0.1 for κ_{org} . The BC volume fraction and $\frac{\sigma_{\kappa_{\text{CCN}}}}{\kappa_{\text{CCN}}}$ were assumed as 10% and 7%, respectively.

at which overall uncertainty in derived κ_{org} was estimated to be less than 0.04 for the example presented in Figure 5. Equation (6) suggests that the uncertainty weakly depends on the κ_{org} , because κ_{inorg} is typically much larger than κ_{org} , and the quantity $(\kappa_{\text{inorg}} - \kappa_{\text{org}})$ is insensitive to the value of κ_{org} . As a result, everything else being equal, we expect a larger relative uncertainty in κ_{org} for smaller κ_{org} values, as $\sigma_{\kappa_{\text{org}}}$ is essentially independent of κ_{org} .

5. Results

5.1. Hygroscopicity of Activated Particles

[24] The hygroscopicity of size selected CCN with diameter between 97 and 165 nm ranged from 0.05 to 0.4, in agreement with the range derived from CCN measurements onboard NOAA WP-3D during CalNex [Moore *et al.*, 2012]. The variation in particle hygroscopicity reflects the variations in both organic volume fraction and κ_{org} . From May to August in 2011, particle GF was measured using a Differential Aerosol Sizing and Hygroscopicity Spectrometer Probe (DASH-SP) on the Caltech campus, and particle κ values derived from the measured GF ranged from 0.15 to 0.51 [Hersey *et al.*, 2011], with high values associated with aerosols with very low organics mass fraction (i.e., down to nearly 0%), which were not observed during this study. Similar range for particle hygroscopicity was also observed in other urban areas [Lance *et al.*, 2012; Padro *et al.*, 2012]. The hygroscopicity of size selected CCN was averaged for sizes ranging from 97 to 165 nm, and the diurnal variation over weekdays is shown in Figure 6a. Median and mean hygroscopicities were essentially the same, and both showed a narrow range from 0.16 to 0.24. There was a slight decrease of κ_{CCN} from 8:00 to 16:00, likely due to the increasing organics volume fraction during this period. Diurnal variations in particle hygroscopicity were observed in previous studies and were similarly attributed to variation in the volume fractions of hygroscopic species, such as sulfate [Bougiatioti *et al.*, 2011; Cerully *et al.*, 2011; Lance *et al.*, 2012]. The statistics show

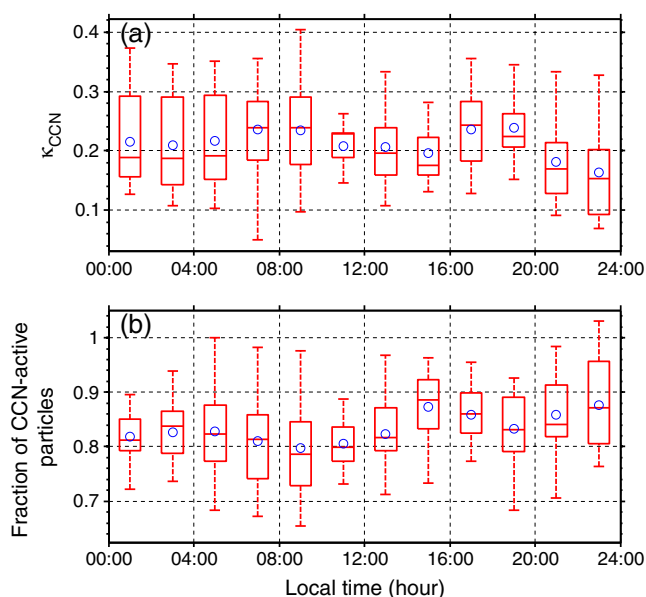


Figure 6. The weekday diurnal variation of (a) the hygroscopicity of CCN active particles ranging from 97 to 165 nm and (b) maximum activation fraction of size selected particles from 97 to 165 nm. The ends of the whiskers represent the minimum and maximum of data expect for the outlines, which are defined as points outside of $\pm 2.7\sigma$. The bottom and the top of the box are the 25th and 75th percentiles, the line inside the box is the 50th percentile (the median), and the blue circle represents the mean value.

relatively narrow ranges of κ_{CCN} in the afternoon compared to those obtained during the morning and evening traffic hours, suggesting a more consistent κ_{CCN} for more aged aerosols, as is further discussed in section 5.2. Figure 6b shows the diurnal variation of E for particles ranging from 97 to 165 nm, which exhibited similar feature as that of OA fraction shown in Figure 3c, suggesting that condensation of SOA was one the main processes that converted hydrophobic particles to hydrophilic ones. During morning and evening traffic hours (i.e., 5:00 to 8:00 and 17:00 to 19:00), slight decreases in both mean and median values of E were observed, and likely due to freshly emitted hydrophobic particles. The slight decreases in E are consistent with the relative minor influence of the local traffic when compared to the pollution plume from LA [Hayes *et al.*, 2012]. The increase in E from 8:00 to 12:00 again indicates that the hydrophobic particles were converted to hydrophilic by condensation of secondary hygroscopic species, including nitrate and SOA, which are consistent with earlier studies [Riemer *et al.*, 2004; Moffet and Prather, 2009; Riemer *et al.*, 2009; Wang *et al.*, 2010]. In contrast, E was relatively constant following the evening traffic hours, because coagulation, the main mechanism to convert particles from hydrophobic to hydrophilic in the absence of photochemistry, is much less effective than the condensation of secondary hygroscopic species during daytime [Riemer *et al.*, 2004; Riemer *et al.*, 2009].

5.2. Hygroscopicity Dispersion and Mixing State of Ambient Aerosol as Functions of Photochemical Age

[25] About 85% of the particles ranging from 97 nm to 165 nm had $\sigma(\kappa)/\bar{\kappa}$ values between 0.3 to 1, consistent with

the ranges previously observed in urban environment [Su *et al.*, 2010; Padro *et al.*, 2012], Similar ranges were also found in the remote Boreal forests of Hyttälä, Finland [Cerully *et al.*, 2011], and at Finokalia, Crete, where a diversity of air masses were sampled [Bougiatioti *et al.*, 2011]. The variation of $\sigma(\kappa)/\bar{\kappa}$ was examined as a function of photochemical age, which was derived as the equivalent exposure time to OH with a concentration of $5 \times 10^6 \text{ cm}^{-3}$, representative for the afternoons of clear days [Washenfelder *et al.*, 2011]. The photochemical age was determined from the measured ratio between two hydrocarbons, benzene and 1,2,4-trimethyl benzene, that were emitted at a constant ratio from mobile sources but removed by OH at very different rates [de Gouw *et al.*, 2005; Borbon *et al.*, 2012]. The photochemical age of air mass was binned into half an hour intervals, and the mean and standard deviation of the dispersion for each photochemical age bin are presented in Figure 7a. The dispersions derived using the two different fitting functions are essentially the same and decreased with increasing photochemical age. This is consistent with the picture that as particles age in the atmosphere through condensation of secondary species and coagulation, the compositions of particles at given sizes become increasingly similar. In about 7 h, the hygroscopicity dispersion decreased to 0.2, which is essentially the same as that of pure ammonium sulfate calibration particles (Note, even for the pure ammonium sulfate particles, that the measured dispersion is greater than zero due to width of DMA transfer function and other non-idealities). This is in agreement with earlier results that within a few hours during daytime, aerosol particles become sufficiently internally mixed such that they may be treated as internal mixtures for calculating CCN concentrations [Wang *et al.*, 2010]. It is worth noting that for most of the measurements, the derived hygroscopicity dispersion was much larger than 0.2, suggesting the gradual increase of R_a with S was mainly due to heterogeneity in particle hygroscopicity.

[26] The maximum activated fraction initially increased with increasing photochemical age and quickly reached a plateau of $\sim 100\%$ in 3–4 h (Figure 7b). This indicates that the initially nonhygroscopic particles quickly became hygroscopic and nearly every particle could serve as CCN at $S \sim 0.4\%$ in just a few hours. As the photochemical age was based on OH concentration that is representative for afternoons of clear days, this aging process is expected to take somewhat longer time during night. The finding is consistent with earlier results that the timescales for the conversion of hydrophobic POA and BC to hydrophilic particles during daytime in urban environment is substantially shorter than the 1–2 days used in some global models [Riemer *et al.*, 2004; Moffet and Prather, 2009; Wang *et al.*, 2010].

5.3. κ_{org} Derived from Particle Hygroscopicity and Composition

[27] As described earlier, for derivation of κ_{org} , measurements were averaged into periods ranging from 2.6 to 9.0 h to increase signal-to-noise ratio (SNR) and reduce the uncertainty in derived κ_{org} . These averaging periods, which are a minimum of 2 h in duration, were identified using the following criteria:

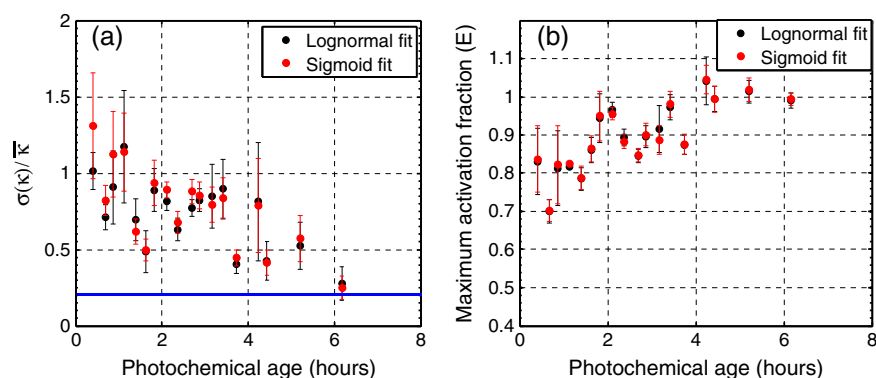


Figure 7. The dependence of (a) hygroscopicity dispersion and (b) maximum activated fraction (E) on photochemical age. The blue solid line in plot (a) represents the derived hygroscopicity dispersion (0.2) for $(\text{NH}_4)_2\text{SO}_4$ calibration aerosols.

[28] 1. The variation in bulk organic volume fraction (i.e., the difference between the maximum and minimum) was less than 10% during the averaging period. This criterion was to ensure essentially constant particle composition, and therefore hygroscopicity, during the periods such that data could be averaged to increase signal to noise ratio or counting statistics.

[29] 2. The average bulk organic volume fraction was no less than 60% during the period, because the uncertainty in derived κ_{org} increased rapidly with decreasing x_{org} (Figure 5).

[30] The above criteria led to a total of 10 periods. The derivation of the κ_{org} was also focused on cases when a vast majority of size-selected particles were CCN active (i.e., E greater than 85%), and the size-selected CCN exhibited similar hygroscopicity (i.e., dispersion in hygroscopicity is less than 1). This was to reduce the impact on the derived κ_{org} by the assumptions that externally mixed CCN-inactive particles consist of BC only and that all CCN have the same composition. As described earlier, for each period, the analysis focused on four sizes ranging from 126 nm to 180 nm where both the counting statistics of size-resolved CCN measurements (based on aerosol number) and the signal to noise ratio of the AMS measurements (aerosol mass based) were reasonable. κ_{org} derived from these cases ranged from 0.05 to 0.23 with an average value of 0.13, in agreement with an earlier study in Pasadena [Hersey et al., 2011]. These values are also consistent with the results from

earlier smog chamber studies, which showed the hygroscopicity ranged from 0.04 to 0.14 for SOA formed from both biogenic and anthropogenic VOC precursors [Prenni et al., 2007; Duplissy et al., 2008; Engelhart et al., 2008; Wex et al., 2009]. Ambient SOA can become more aged than typical chamber SOA [Aiken et al., 2008], consistent with the larger κ_{org} derived from the data collected during CalNex.

5.4. Relationship Between κ_{org} and Organic Oxidation Level

[31] Given the variation of κ_{org} and its impact on simulated CCN concentrations, efficient parameterizations that can capture the major causes of variation of κ_{org} are essential for implementation in large scale models. One promising idea is that κ_{org} may be parameterized based on the organic oxidation level, which can be measured by aerosol mass spectrometry (i.e., O : C atomic ratio). Figure 8a shows the variation of derived κ_{org} as a function of O : C. The size-resolved O : C was estimated using the relationship $\text{O} : \text{C} = 3.25(f_{44}) + 0.001$, where f_{44} is the fraction of the total organic signal at m/z 44 [Hayes et al., 2012]. The uncertainty of derived κ_{org} was calculated using the approach described earlier. The precision of O : C estimated from measurements by the same AMS is 3% [Aiken et al., 2008], and the inter-instrument variability for estimated O : C is $\sim 10\%$. As the results are compared to earlier studies during which O : C was also derived from AMS measurements, the uncertainty in

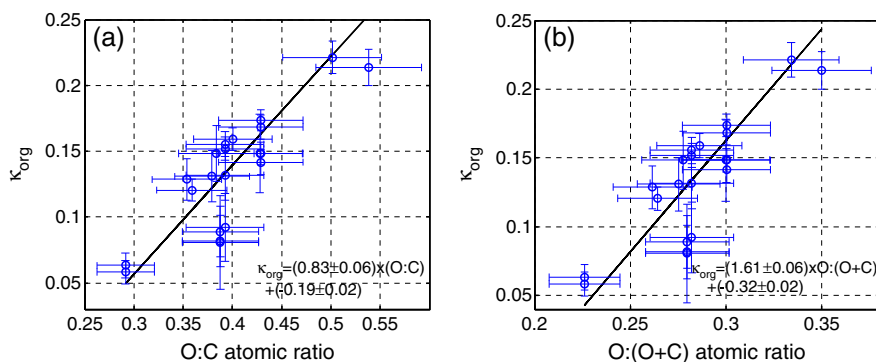


Figure 8. Derived organic hygroscopicity as a function of (a) O : C atomic ratio and (b) O : (O + C) atomic ratio and least squares fits.

derived O:C was estimated as 10% [Hayes *et al.*, 2012]. Consistent with earlier studies, κ_{org} increased as organics became more oxidized (i.e., higher O:C value). A least squares fit of data that taking into consideration of both uncertainties in derived κ_{org} and O:C yielded $\kappa_{\text{org}} = (0.83 \pm 0.06) \times (\text{O:C}) + (-0.19 \pm 0.02)$. The Pearson R^2 was 0.71, suggesting most of the variation in κ_{org} observed during CalNex could be explained by the variation in organics oxidation level. It is worth noting that the overall hygroscopicity of a mixture is the volume average of hygroscopicity of participating species. However, the O:C atomic ratio of a mixture cannot be derived as the volume average of the O:C of its components. Therefore, a linear relationship between κ_{org} and O:C, as derived from nearly all previous studies, is not self-consistent. A more consistent approach is to fit κ_{org} as a linear function of O:(O+C), which yielded $\kappa_{\text{org}} = (1.61 \pm 0.06) \times \text{O}:(\text{O}+\text{C}) + (-0.32 \pm 0.02)$ (Figure 8b) with Pearson R^2 value of 0.70. We note that high R^2 values were achieved by fitting to either O:C or O:(O+C), likely due to the relatively narrow range of O:C observed during this study. For a wide range of O:C, a higher R^2 value would be expected when fitting κ_{org} to O:(O+C).

[32] The relationship between κ_{org} and O:C is compared to results from earlier studies during which κ_{org} was derived under both sub-saturated conditions using HTDMA (Figure 9a) and supersaturated conditions using CCN measurements (Figure 9b). The relationship derived from this study agrees well with that based on HTDMA measurements of SOA formed from 1,3,5-trimethylbenzene (TMB), a surrogate for anthropogenic precursors, in a smog chamber [Duplissy *et al.*, 2011]. At the same O:C, κ_{org} of SOA formed from TMB is substantially higher than that of SOA formed from representative biogenic precursors including isoprene and α -pinene. One possible explanation is that for SOA from TMB photooxidation, the acids present in the aerosol are mainly mono-acids, while the acids found in the SOA from α -pinene or isoprene photooxidation are approximately half mono- and half di-acids [Duplissy

et al., 2011]. The agreement with results of SOA formed from TMB is consistent with that the CalNex-LA site was more of a receptor site for pollution from downtown LA, and SOA formed from anthropogenic precursors contributed substantially to the total OA concentration [Zhang *et al.*, 2011; Bahreini *et al.*, 2012].

[33] Chang *et al.* [2010] studied κ_{org} based on CCN measurements at a rural site in Ontario, Canada. To the best of our knowledge, this is the only previous study that examined the relationship between κ_{org} and O:C based on field CCN measurements. The best fit from their results suggest smaller κ_{org} at low O:C value and steeper increase in κ_{org} with increasing O:C. However, as the result was based on total CCN measurement (i.e., not size-resolved), the uncertainty in the derived relationship was quite high ($\kappa_{\text{org}} = (0.9 \pm 0.5) \times (\text{O:C}) - (0.3 \pm 0.2)$, $0.3 < \text{O:C} < 0.6$), which may partially explain the difference between the studies. Massoli *et al.* [2010] and Lambe *et al.* [2011] examined the hygroscopicity of SOA and oxidized POA (OPOA) formed in laboratory experiments from the oxidation of a range of precursors representing atmospherically relevant biogenic and anthropogenic sources. The SOA and OPOA particles were generated via controlled exposure of precursors to OH radicals and/or O_3 in a Potential Aerosol Mass (PAM) flow reactor over timescales equivalent to 1–20 days of atmospheric aging resulting in O:C values ranging from 0.05 to 1.42. While the results from this study and those based on the laboratory measurements overlap in the range of O:C 0.35–0.45, κ_{org} derived from this study exhibits stronger increase with increasing O:C (i.e., larger slope from the least squares fit). At higher O:C values over ~ 0.5 , κ_{org} derived here is substantially higher than the PAM results. It is worth noting that the current AMS data analysis software only allows derivation of bulk O:C through high resolution analysis of mass spectrum obtained in Mass Spectrum (MS) mode operation (i.e., bulk measurements). This approach was employed by Massoli *et al.* [2010] and Lambe *et al.* [2011] to derive bulk O:C, which should represent O:C at various CCN sizes, because no substantial O:C dependence on

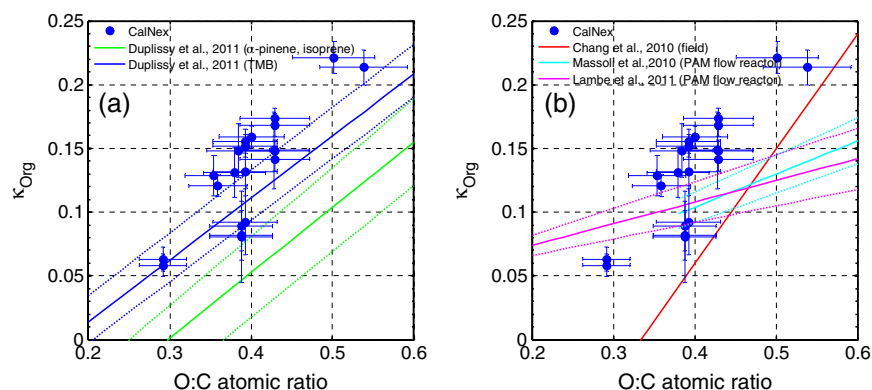


Figure 9. Comparison of the relationship between organic hygroscopicity and O:C atomic ratio derived from this study to earlier results. The solid and dashed lines represent best fit and range of the previous results. (a) Comparison to organic hygroscopicity derived from HTDMA measurements of SOA formed from α -pinene, isoprene, and TMB (trimethylbenzene) generated in a smog chamber [Duplissy *et al.*, 2011], (b) comparison to results based on CCN measurements at Egbert, Ontario Canada, [Chang *et al.*, 2010] and of SOA and oxidized POA (OPOA) generated via controlled exposure of precursors to OH radicals and/or O_3 in Potential Aerosol Mass (PAM) flow reactors [Massoli *et al.*, 2010; Lambe *et al.*, 2011]. The linear fit of the data presented in Massoli *et al.* [2010] is reported in Lambe *et al.* [2011].

particle size is expected for organic aerosols formed in the PAM reactor. For this study, O:C at CCN sizes was derived from size-resolved f_{44} (obtained from PToF data) using the relationship between O:C and f_{44} . The relationship was characterized using the method described in *Aiken et al.* [2008] and was based on the bulk O:C and f_{44} derived from MS mode data collected during this study. This approach was used to derive O:C from f_{44} for some of the results presented in *Lambe et al.* [2011]. Therefore, we expect O:C values derived in this study and *Lambe et al.* [2011] are reasonably accurate. *Chang et al.* [2010] derived O:C employing a relationship between O:C and f_{44} reported in an earlier study [*Aiken et al.*, 2008], which might not be accurate for the aerosol observed. The steeper slope reported by *Chang et al.* [2010] might be in part due to the uncertainty in the derived O:C value.

[34] The range of OA mass loading during this study was from 2 to 25 $\mu\text{g}/\text{m}^3$, which was within the range of 1 to 100 $\mu\text{g}/\text{m}^3$ studied by *Massoli et al.* [2010]. In addition, the relationship between κ_{org} and O:C reported by *Massoli et al.* [2010] exhibited little dependence on organic mass loading. Therefore, the differences in the relationships between κ_{org} and O:C among the studies could not be explained by the variations in organic mass loading and may be due to the differences in organics composition between ambient organic aerosols observed in this study and those formed in smog chamber or PAM reactor. For example, cloud processing and aqueous chemistry in wet aerosols may contribute substantially to SOA formation, while SOA are mainly formed through gas phase reactions in smog chamber or PAM reactor. This may lead to different SOA compounds and therefore the relationship between κ_{org} and O:C. Another possible reason is that the concentrations of oxidants inside PAM are several orders of magnitude higher than observed in the ambient atmosphere, which could also lead to different compounds in the SOA formed. The discrepancy suggests that more results on κ_{org} derived from ambient aerosols are needed to better understand and represent organics hygroscopicity in climate models.

6. Conclusions

[35] During the CalNex campaign, aerosol CCN activation properties and chemical composition were characterized at an urban supersite in Pasadena, California, from 15 May to 4 June 2010. Monodisperse aerosol particles ranging from 20 to 350 nm were first classified using a differential mobility analyzer (DMA). The activated fraction of the classified aerosol, defined as the ratio of its CCN concentration (characterized by a CCN counter) to total CN concentration (measured by a condensation particle counter), was derived as a function of both particle size and supersaturation, which ranged from 0.1% to 0.4%. Aerosol chemical composition was measured using an AMS. Increases in aerosol mode diameter, organics mass loading, and aerosol organics volume fraction were typically observed from 12:00 to 18:00. These increases are attributed to advection of SOA formed in the downtown LA plume through photochemical reactions. The hygroscopicity of CCN-active particles with diameter from 97 to 165 nm, derived from the size-resolved activated fraction, ranged from 0.05

to 0.4. The derived hygroscopicity dispersion decreased with increasing photochemical age, consistent with the picture that as particles age in the atmosphere through coagulation and condensation of secondary species, the compositions of particles at given sizes become increasingly similar. During daytime, in about 7 h, the hygroscopicity dispersion decreased to 0.2, which is essentially the same as that of pure ammonium sulfate calibration particles. This is in agreement with early results that in urban environment, aerosol particles quickly become sufficiently internally mixed such that they may be treated as internal mixture for calculating CCN concentrations [*Wang et al.*, 2010]. The maximum activated fraction of size selected particles increased to near 100% at photochemical age of 3–4 h, indicating that the initially hydrophobic particles quickly became hydrophilic as a result of condensation of secondary hygroscopic species. During daytime, nearly every particle became efficient CCN in just a few hours.

[36] Based on the particle hygroscopicity and aerosol chemical composition, the organic hygroscopicity (κ_{org}) was derived and ranged from 0.05 to 0.23 with an average value of 0.13. The uncertainty in derived κ_{org} was dominated by the uncertainties in measured CCN particle hygroscopicity and the volume fraction of organics. The uncertainty in derived κ_{org} decreased rapidly with increasing x_{org} . As a result, the analysis of κ_{org} was focused on periods with high organic volume fraction ($x_{\text{org}} > 60\%$). The derived κ_{org} generally increased with the organic oxidation level, and most of the variation (71%) in κ_{org} could be explained by the variation of the O:C atomic ratio alone. The least squares fit taking into consideration the uncertainties in both derived κ_{org} and O:C atomic ratio yielded $\kappa_{\text{org}} = (0.83 \pm 0.06) \times (\text{O:C}) + (-0.19 \pm 0.02)$. This relationship agrees very well with that based on HTDMA measurements of SOA formed from trimethylbenzene (TMB), a surrogate for anthropogenic precursors, in a smog chamber. The agreement is consistent with that the CalNex-LA site was principally a receptor site for pollution from downtown LA, and anthropogenic VOCs as dominant SOA precursors [*Zhang et al.*, 2011; *Bahreini et al.*, 2012]. Compared to previous results based on CCN measurements of aerosols generated in PAM reactors, κ_{org} derived here exhibits stronger increase with O:C and therefore substantially higher values when $\text{O:C} > \sim 0.5$. This discrepancy is likely due to the differences in organic compositions between ambient organic aerosols observed in this study and those formed in PAM reactors.

[37] **Acknowledgments.** This research was performed with support from the Office of Biological and Environmental Research under contract number DE-AC02-98CH10866. We acknowledge Caltech for hosting the supersite and logistics support from California Air Resources Board, NOAA, and UCLA. The authors acknowledge the US Department of Energy ARM program for providing some of instruments deployed in this study. Patrick L. Hayes and Jose L. Jimenez thank CARB 08-319/11-305 and DOE (BER/ASR) DE-SC0006035 and DE-FG02-11ER65293, as well as a CIRES Visiting Fellowship to Patrick L. Hayes. The SP2 data were supported by the UK National Environment Research Council project Multiscale Chemical Composition of Carbonaceous particles and Coatings (MC4) [Grant ref: NE/H008136/1]. The University of Manchester activities were supported by The UK Natural Environment Research Council through a PhD studentship and the project Multiscale Chemical Composition of Carbonaceous particles and Coatings (MC4) [Grant ref: NE/H008136/1].

References

- Abhatt, J. P. D., K. Broekhuizen, and P. P. Kumal (2005), Cloud condensation nucleus activity of internally mixed ammonium sulfate/organic acid aerosol particles, *Atmos. Environ.*, *39*, 4767–4778.
- Aiken, A. C., P. F. DeCarlo, and J. L. Jimenez (2007), Elemental analysis of organic species with electron ionization high-resolution mass spectrometry, *Anal. Chem.*, *79*, 8350–8358.
- Aiken, A. C., et al. (2008), O/C and OM/OC ratios of primary, secondary, and ambient organic aerosols with high-resolution time-of-flight aerosol mass spectrometry, *Environ. Sci. Technol.*, *42*, 4478–4485.
- Albrecht, B. A. (1989), Aerosols, cloud microphysics, and fractional cloudiness, *Science*, *245*, 1227–1230.
- Asa-Awuku, A., et al. (2009), Relating CCN activity, volatility, and droplet growth kinetics of beta-carophyllene secondary organic aerosol, *Atmos. Chem. Phys.*, *9*, 795–812.
- Asa-Awuku, A., et al. (2010), Water-soluble SOA from Alkene ozonolysis: Composition and droplet activation kinetics inferences from analysis of CCN activity, *Atmos. Chem. Phys.*, *10*, 1585–1597, doi:10.5194/acp-10-1585-2010.
- Bahreini, R., et al. (2012), Gasoline emissions dominate over diesel in formation of secondary organic aerosol mass, *Geophys. Res. Lett.*, *39*, L06805, doi:10.1029/2011GL050718.
- Bilde, M., and B. Svenningsson (2004), CCN activation of slightly soluble organics: the importance of small amounts of inorganic salt and particle phase, *Tellus B*, *56*, 128–134.
- Bond, T. C., and R. W. Bergstrom (2006), Light absorption by carbonaceous particles: An investigative review, *Aerosol Sci. Tech.*, *40*, 27–67.
- Borbon, A., et al. (2012), Emissions of anthropogenic VOCs in northern mid-latitude megacities: Observations vs. emission inventories in Los Angeles and Paris, *J. Geophys. Res.*, *In Press*, doi:10.1029/2012JD018235.
- Bougiatioti, A., et al. (2011), Size-resolved CCN distributions and activation kinetics of aged continental and marine aerosol, *Atmos. Chem. Phys.*, *11*, 8791–8808, doi:10.5194/acp-11-8791-2011.
- Cerully, K. M., et al. (2011), Aerosol hygroscopicity and CCN activation kinetics in a boreal forest environment during the 2007 EUCAARI campaign, *Atmos. Chem. Phys.*, *11*, 12369–12386, doi:10.5194/acp-11-12369-2011.
- Chang, R. Y. W., et al. (2010), The hygroscopicity parameter (κ) of ambient organic aerosol at a field site subject to biogenic and anthropogenic influences: Relationship to degree of aerosol oxidation, *Atmos. Chem. Phys.*, *10*, 5047–5064.
- Charlson, R. J., et al. (2001), Atmospheric science—Reshaping the theory of cloud formation, *Science*, *292*, 2025–2026.
- Collins, D. R., R. C. Flagan, and J. H. Seinfeld (2002), Improved inversion of scanning DMA data, *Aerosol Sci. Tech.*, *36*, 1–9.
- Cross, E. S., et al. (2007), Laboratory and ambient particle density determinations using light scattering in conjunction with aerosol mass spectrometry, *Aerosol Sci. Tech.*, *41*, 343–359.
- Cubison, M. J., et al. (2008), The influence of chemical composition and mixing state of Los Angeles urban aerosol on CCN number and cloud properties, *Atmos. Chem. Phys.*, *8*, 5649–5667.
- de Gouw, J. A., et al. (2005), Budget of organic carbon in a polluted atmosphere: Results from the New England Air Quality Study in 2002, *J. Geophys. Res.*, *110*, D16305, doi:10.1029/2004JD005623.
- DeCarlo, P. F., et al. (2006), Field-deployable, high-resolution, time-of-flight aerosol mass spectrometer, *Anal. Chem.*, *78*, 8281–8289.
- DeCarlo, P. F., et al. (2004), Particle morphology and density characterization by combined mobility and aerodynamic diameter measurements. Part 1: Theory, *Aerosol Sci. Tech.*, *38*, 1185–1205.
- Duplissy, J., et al. (2011), Relating hygroscopicity and composition of organic aerosol particulate matter, *Atmos. Chem. Phys.*, *11*, 1155–1165, doi:10.5194/acp-11-1155-2011.
- Duplissy, J., et al. (2008), Cloud forming potential of secondary organic aerosol under near atmospheric conditions, *Geophys. Res. Lett.*, *35*, L03818.
- Engelhart, G. J., A. Asa-Awuku, A. Nenes, and S. N. Pandis (2008), CCN activity and droplet growth kinetics of fresh and aged monoterpene secondary organic aerosol, *Atmos. Chem. Phys.*, *8*, 3937–3949.
- Ervens, B., et al. (2010), CCN predictions using simplified assumptions of organic aerosol composition and mixing state: A synthesis from six different locations, *Atmos. Chem. Phys.*, *10*, 4795–4807.
- Facchini, M. C., M. Mircea, S. Fuzzi, and R. J. Charlson (1999), Cloud albedo enhancement by surface-active organic solutes in growing droplets, *Nature*, *401*, 257–259.
- Frank, G. P., U. Dusek, and M. O. Andreae (2006), Technical note: A method for measuring size-resolved CCN in the atmosphere, *Atmos. Chem. Phys. Discuss.*, *6*, 4879–4895.
- Good, N., et al. (2010), Consistency between parameterisations of aerosol hygroscopicity and CCN activity during the RHaMBLE discovery cruise, *Atmos. Chem. Phys.*, *10*, 3189–3203.
- Gunthe, S. S., et al. (2009), Cloud condensation nuclei in pristine tropical rainforest air of Amazonia: Size-resolved measurements and modeling of atmospheric aerosol composition and CCN activity, *Atmos. Chem. Phys.*, *9*, 7551–7575.
- Hartz, K. E. H., et al. (2005), Cloud condensation nuclei activation of monoterpene and sesquiterpene secondary organic aerosol, *J. Geophys. Res.*, *110*, D14208.
- Hayes, P. L., et al. (2012), Aerosol composition and sources in Los Angeles during the 2010 CalNex campaign, *J. Geophys. Res.*, Submitted.
- Hegg, D. A., et al. (2001), Laboratory studies of the efficiency of selected organic aerosols as CCN, *Atmos. Res.*, *58*, 155–166.
- Hersey, S. P., et al. (2011), The Pasadena Aerosol Characterization Observatory (PACO): Chemical and physical analysis of the Western Los Angeles basin aerosol, *Atmos. Chem. Phys.*, *11*, 7417–7443, doi:10.5194/acp-11-7417-2011.
- Hudson, J. G., and X. Y. Da (1996), Volatility and size of cloud condensation nuclei, *J. Geophys. Res.*, *101*, 4435–4442.
- Huff-Hartz, K. E. H., et al. (2006), Cloud condensation nuclei activation of limited solubility organic aerosol, *Atmos. Environ.*, *40*, 605–617.
- IPCC (2007), Climate Change 2007—The Physical Science Basis: Contribution of Working Group I to the Fourth Assessment Report of the IPCC, 2, pp. 136, Cambridge University Press, New York.
- Irwin, M., et al. (2011), Size-resolved aerosol water uptake and cloud condensation nuclei measurements as measured above a Southeast Asian rainforest during OP3, *Atmos. Chem. Phys.*, *11*, 11157–11174, doi:10.5194/acp-11-11157-2011.
- Jacobson, M. Z. (2001), Global direct radiative forcing due to multicomponent anthropogenic and natural aerosols, *J. Geophys. Res.*, *106*, 1551–1568, doi:10.1029/2000JD900514.
- Jimenez, J. L., et al. (2009), Evolution of organic aerosols in the atmosphere, *Science*, *326*, 1525–1529.
- Kammermann, L., et al. (2010), Subarctic atmospheric aerosol composition: 3. Measured and modeled properties of cloud condensation nuclei, *J. Geophys. Res.*, *115*, D04202, doi:10.1029/2009JD012447.
- Kanakidou, M., et al. (2005), Organic aerosol and global climate modelling: A review, *Atmos. Chem. Phys.*, *5*, 1053–1123.
- Kang, E., M. J. Root, D. W. Toohey, and W. H. Brune (2007), Introducing the concept of Potential Aerosol Mass (PAM), *Atmos. Chem. Phys.*, *7*, 5727–5744, doi:10.5194/acp-7-5727-2007.
- King, S. M., et al. (2007), Cloud condensation nucleus activity of secondary organic aerosol particles mixed with sulfate, *Geophys. Res. Lett.*, *34*, L24806, doi:10.1029/2007GL030390.
- King, S. M., et al. (2009), Increased cloud activation potential of secondary organic aerosol for atmospheric mass loadings, *Atmos. Chem. Phys.*, *9*, 2959–2971.
- Köhler, H. (1936), The nucleus in and the growth of hygroscopic droplets, *Trans. Farad. Soc.*, *32*, 1152–1161.
- Kumar, P. P., K. Broekhuizen, and J. P. D. Abbatt (2003), Organic acids as cloud condensation nuclei: Laboratory studies of highly soluble and insoluble species, *Atmos. Chem. Phys.*, *3*, 509–520.
- Kuwata, M., S. R. Zorn, and S. T. Martin (2012), Using elemental ratios to predict the density of organic material composed of carbon, hydrogen, and oxygen, *Environ. Sci. Technol.*, *46*, 787–794.
- Laaksonen, A., P. Korhonen, M. Kulmala, and R. J. Charlson (1998), Modification of the Köhler equation to include soluble trace gases and slightly soluble substances, *J. Atmos. Sci.*, *55*, 853–862.
- Lambe, A. T., et al. (2011), Laboratory studies of the chemical composition and cloud condensation nuclei (CCN) activity of secondary organic aerosol (SOA) and oxidized primary organic aerosol (OPOA), *Atmos. Chem. Phys.*, *11*, 8913–8928, doi:10.5194/acp-11-8913-2011.
- Lance, S. (2007), Quantifying compositional impacts of ambient aerosol on cloud droplet formation, PhD Thesis, Georgia Institute of Technology, Atlanta.
- Lance, S., J. Medina, J. N. Smith, and A. Nenes (2006), Mapping the operation of the DMT Continuous Flow CCN counter, *Aerosol Sci. Tech.*, *40*, 242–254.
- Lance, S., et al. (2012), Aerosol mixing-state, hygroscopic growth and cloud activation efficiency during MIRAGE 2006, *Atmos. Chem. Phys. Discuss.*, *12*, 15709–15742, doi:10.5194/acpd-12-15709-2012.
- Liu, D., et al. (2010), Single particle characterization of black carbon aerosols at a tropospheric alpine site in Switzerland, *Atmos. Chem. Phys.*, *10*, 7389–7407.
- Liu, X., et al. (2008), Indirect effect in NCAR CAM: Sensitivity to aerosol-cloud parameterizations, *Eos Trans. AGU*, *89(53)*, Fall Meet. Suppl., Abstract A32A-03.

- Liu, X., and J. Wang (2010), How important is organic aerosol hygroscopicity to aerosol indirect forcing? *Environ. Res. Lett.*, *5*, doi:10.1088/1748-9326/5/4/044010.
- Lohmann, U., et al. (2004), How efficient is cloud droplet formation of organic aerosols?, *Geophys. Res. Lett.*, *31*, L05108.
- Malloy, Q. G. J., et al. (2009), Real-time aerosol density determination utilizing a modified scanning mobility particle sizer—Aerosol particle mass analyzer system, *Aerosol Sci. Tech.*, *43*, 673–678.
- Massoli, P., et al. (2010), Relationship between aerosol oxidation level and hygroscopic properties of laboratory generated secondary organic aerosol (SOA) particles, *Geophys. Res. Lett.*, *37*, L24801, doi:10.1029/2010GL045258.
- McFiggans, G., et al. (2006), The effect of physical and chemical aerosol properties on warm cloud droplet activation, *Atmos. Chem. Phys.*, *6*, 2593–2649.
- McMeeking, G. R., et al. (2010), Black carbon measurements in the boundary layer over western and northern Europe, *Atmos. Chem. Phys.*, *10*, 9393–9414.
- Mircea, M., et al. (2002), The influence of the organic aerosol component on CCN supersaturation spectra for different aerosol types, *Tellus B*, *54*, 74–81.
- Mochida, M., et al. (2010), Size-segregated measurements of cloud condensation nucleus activity and hygroscopic growth for aerosols at Cape Hedo, Japan, in spring 2008, *J. Geophys. Res.*, *115*, D21207, doi:10.1029/2009JD013216.
- Moffet, R. C., and K. A. Prather (2009), In-situ measurements of the mixing state and optical properties of soot with implications for radiative forcing estimates, *Proc. Natl. Acad. Sci. USA*, *106*, 11872–11877.
- Moore, R. H., et al. (2012), Hygroscopicity and composition of California CCN during summer 2010, *J. Geophys. Res.*, *117*, doi:10.1029/2011JD017352.
- Moore, R. H., A. Nenes, and J. Medina (2010), Scanning mobility CCN analysis—A method for fast measurements of size-resolved CCN distributions and activation kinetics, *Aerosol Sci. Tech.*, *44*, 861–871, doi:10.1080/02786826.2010.498715.
- Nenes, A., et al. (2002), Can chemical effects on cloud droplet number rival the first indirect effect?, *Geophys. Res. Lett.*, *29*, 1848.
- Padro, L. T., et al. (2012), Mixing state and compositional effects on CCN activity and droplet growth kinetics of size-resolved CCN in an urban environment, *Atmos. Chem. Phys.*, *12*, 10239–10255, doi:10.5194/acp-12-10239-2012.
- Padro, L. T., et al. (2010), Investigation of cloud condensation nuclei properties and droplet growth kinetics of the water-soluble aerosol fraction in Mexico City, *J. Geophys. Res.*, *115*, D09204, doi:10.1029/2009JD013195.
- Park, K., D. B. Kittelson, M. R. Zachariah, and P. H. McMurry (2004), Measurement of inherent material density of nanoparticle agglomerates, *J. Nanopart. Res.*, *6*, 267–272.
- Petters, M. D., et al. (2009a), Cloud condensation nucleation activity of biomass burning aerosol, *J. Geophys. Res.*, *114*, D22205, doi:10.1029/2009JD012353.
- Petters, M. D., and S. M. Kreidenweis (2007), A single parameter representation of hygroscopic growth and cloud condensation nucleus activity, *Atmos. Chem. Phys.*, *7*, 1961–1971.
- Petters, M. D., and S. M. Kreidenweis (2008), A single parameter representation of hygroscopic growth and cloud condensation nucleus activity—Part 2: Including solubility, *Atmos. Chem. Phys.*, *8*, 6273–6279.
- Petters, M. D., A. J. Prenni, S. M. Kreidenweis, and P. J. DeMott (2007), On measuring the critical diameter of cloud condensation nuclei using mobility selected aerosol, *Aerosol Sci. Tech.*, *41*, 907–913.
- Petters, M. D., et al. (2009b), Towards closing the gap between hygroscopic growth and activation for secondary organic aerosol—Part 2: Theoretical approaches, *Atmos. Chem. Phys.*, *9*, 3999–4009.
- Prenni, A. J., et al. (2007), Cloud droplet activation of secondary organic aerosol, *J. Geophys. Res.*, *112*, D10223, doi:10.1029/2006JD007963.
- Raymond, T. M., and S. N. Pandis (2002), Cloud activation of single-component organic aerosol particles, *J. Geophys. Res.*, *107*, 4787, doi:10.1029/2002JD002159.
- Raymond, T. M., and S. N. Pandis (2003), Formation of cloud droplets by multicomponent organic particles, *J. Geophys. Res.*, *108*, 4469, doi:10.1029/2003JD003503.
- Reutter, P., et al. (2009), Aerosol- and updraft-limited regimes of cloud droplet formation: Influence of particle number, size and hygroscopicity on the activation of cloud condensation nuclei (CCN), *Atmos. Chem. Phys.*, *9*, 7067–7080.
- Riemer, N., H. Vogel, and B. Vogel (2004), Soot aging time scales in polluted regions during day and night, *Atmos. Chem. Phys.*, *4*, 1885–1893.
- Riemer, N., M. West, R. A. Zaveri, and R. C. Easter (2009), Simulating the evolution of soot mixing state with a particle-resolved aerosol model, *J. Geophys. Res.*, *114*, D09202 doi:10.1029/2008JD011073.
- Rissler, J., et al. (2006), Size distribution and hygroscopic properties of aerosol particles from dry-season biomass burning in Amazonia, *Atmos. Chem. Phys.*, *6*, 471–491.
- Rissman, T. A., A. Nenes, and J. H. Seinfeld (2004), Chemical amplification (or dampening) of the Twomey effect: Conditions derived from droplet activation theory, *J. Atmos. Sci.*, *61*, 919–930.
- Roberts, G. C., and A. Nenes (2005), A continuous-flow streamwise thermal-gradient CCN chamber for atmospheric measurements, *Aerosol Sci. Tech.*, *39*, 206–221.
- Rose, D., et al. (2008), Calibration and measurement uncertainties of a continuous-flow cloud condensation nuclei counter (DMT-CCNC): CCN activation of ammonium sulfate and sodium chloride aerosol particles in theory and experiment, *Atmos. Chem. Phys.*, *8*, 1153–1179.
- Rose, D., et al. (2010), Cloud condensation nuclei in polluted air and biomass burning smoke near the mega-city Guangzhou, China—Part 1: Size-resolved measurements and implications for the modeling of aerosol particle hygroscopicity and CCN activity, *Atmos. Chem. Phys.*, *10*, 3365–3383.
- Schwarz, J. P., et al. (2010), The detection efficiency of the single particle soot photometer, *Aerosol Sci. Tech.*, *44*, 612–628.
- Shantz, N. C., et al. (2008), The effect of organic compounds on the growth rate of cloud droplets in marine and forest settings, *Atmos. Chem. Phys.*, *8*, 5869–5887.
- Shulman, M. L., et al. (1996), Dissolution behavior and surface tension effects of organic compounds in nucleating cloud droplets, *Geophys. Res. Lett.*, *23*, 277–280.
- Stephens, M., N. Turner, and J. Sandberg (2003), Particle identification by laser-induced incandescence in a solid-state laser cavity, *Appl. Optics*, *42*, 3726–3736.
- Su, H., et al. (2010), Hygroscopicity distribution concept for measurement data analysis and modeling of aerosol particle mixing state with regard to hygroscopic growth and CCN activation, *Atmos. Chem. Phys.*, *10*, 7489–7503, doi:10.5194/acp-10-7489-2010.
- Sueper, D. (2011), ToF-AMS Analysis Software, University of Colorado, Boulder, Colorado, USA.
- Svenningsson, B., et al. (2006), Hygroscopic growth and critical supersaturations for mixed aerosol particles of inorganic and organic compounds of atmospheric relevance, *Atmos. Chem. Phys.*, *6*, 1937–1952.
- Turpin, B. J., and H. J. Lim (2001), Species contributions to PM_{2.5} mass concentrations: Revisiting common assumptions for estimating organic mass, *Aerosol Sci. Tech.*, *35*, 602–610.
- Twomey, S. (1977), Influence of pollution on shortwave albedo of clouds, *J. Atmos. Sci.*, *34*, 1149–1152.
- VanReken, T. M., N. L. Ng, R. C. Flagan, and J. H. Seinfeld (2005), Cloud condensation nucleus activation properties of biogenic secondary organic aerosol, *J. Geophys. Res.*, *110*, D07206.
- Wang, J. (2007), Effects of spatial and temporal variations in aerosol properties on mean cloud albedo, *J. Geophys. Res.*, *112*, D16201, doi:10.1029/2007JD008565.
- Wang, J., et al. (2010), The importance of aerosol mixing state and size-resolved composition on CCN concentration and the variation of the importance with atmospheric aging of aerosols, *Atmos. Chem. Phys.*, *10*, 7267–7283.
- Wang, J., R. C. Flagan, and J. H. Seinfeld (2003), A differential mobility analyzer (DMA) system for submicron aerosol measurements at ambient relative humidity, *Aerosol Sci. Tech.*, *37*, 46–52.
- Wang, J., et al. (2008), Effects of aerosol organics on cloud condensation nucleus (CCN) concentration and first indirect aerosol effect, *Atmos. Chem. Phys.*, *8*, 6325–6339.
- Wang, S. C., and R. C. Flagan (1990), Scanning electrical mobility spectrometer, *Aerosol Sci. Tech.*, *13*, 230–240.
- Ward, D. S., T. Eidhammer, W. R. Cotton, and S. M. Kreidenweis (2010), The role of the particle size distribution in assessing aerosol composition effects on simulated droplet activation, *Atmos. Chem. Phys.*, *10*, 5435–5447.
- Washenfelder, R. A., et al. (2011), The glyoxal budget and its contribution to organic aerosol for Los Angeles, California, during CalNex 2010, *J. Geophys. Res.*, *116*, D00V02, doi:10.1029/2011JD016314.
- Wex, H., et al. (2007), Hygroscopic growth and measured and modeled critical super-saturations of an atmospheric HULIS sample, *Geophys. Res. Lett.*, *34*, L02818.
- Wex, H., et al. (2009), Towards closing the gap between hygroscopic growth and activation for secondary organic aerosol: Part 1—Evidence from measurements, *Atmos. Chem. Phys.*, *9*, 3987–3997.
- Wex, H., F. Stratmann, D. Topping, and G. McFiggans (2008), The Kelvin versus the Raoult Term in the Kohler Equation, *J. Atmos. Sci.*, *65*, 4004–4016.
- Wonaschutz, A., et al. (2011), Impact of a large wildfire on water-soluble organic aerosol in a major urban area: The 2009 Station Fire in Los Angeles County, *Atmos. Chem. Phys.*, *11*, 8257–8270, doi:10.5194/acp-11-8257-2011.

- Zhang, Q., et al. (2005a), Time- and size-resolved chemical composition of submicron particles in Pittsburgh: Implications for aerosol sources and processes, *J. Geophys. Res.*, *110*, D07S09, doi:10.1029/2004JD004649.
- Zhang, Q., et al. (2007), Ubiquity and dominance of oxygenated species in organic aerosols in anthropogenically-influenced Northern Hemisphere midlatitudes, *Geophys. Res. Lett.*, *34*, L13801, doi:10.1029/2007GL029979.
- Zhang, Q., D. R. Worsnop, M. R. Canagaratna, and J. L. Jimenez (2005b), Hydrocarbon-like and oxygenated organic aerosols in Pittsburgh: Insights into sources and processes of organic aerosols, *Atmos. Chem. Phys.*, *5*, 3289–3311.
- Zhang, X. L., et al. (2011), Light-absorbing soluble organic aerosol in Los Angeles and Atlanta: A contrast in secondary organic aerosol, *Geophys. Res. Lett.*, *38*, L21810, doi:10.1029/2011GL049385.